J. Plasma Physics (1999), *vol.* 61, *part* 4, *pp.* 601–622. Printed in the United Kingdom

Slowly decaying drift turbulence with wave effects

GIOVANNI MANFREDI*
School of Cosmic Physics, Dublin Institute for Advanced Studies, Dublin 2, Ireland

(Received 22 May 1998)

The effect of linear waves on the Charney–Hasegawa–Mima model of drift and geostrophic turbulence is studied numerically for a slowly decaying field. It is shown that wave effects can reduce the efficiency of nonlinear mode coupling, effectively 'freezing' the spectrum to a narrow band in wavenumber space. Selective nonlinear interactions tend to favour velocities parallel to the direction of propagation of the waves. Accordingly, anisotropic spectra are observed, steeper in the direction of wave propagation, and shallower in the perpendicular direction.

1. Introduction

Drift turbulence plays an important role in the physics of strongly magnetized plasmas. It is essentially an electrostatic phenomenon, dominated by macroscopic motion (the $\mathbf{E} \times \mathbf{B}$ and polarization drifts), driven unstable by the presence of temperature gradients. Drift turbulence is also probably responsible, at least in part, for the high level of energy and particle transport observed in tokamaks (anomalous transport, for a review, see Connor and Wilson 1994).

Various models of increasing complexity have been proposed to describe the dynamics of drift turbulence, including fluid models (Manfredi and Ottaviani 1997), gyrokinetic models, both Lagrangian (Sydora et al. 1996) and Eulerian (Manfredi et al. 1996), and gyrofluid models (Waltz et al. 1994). For each type of description, slab, cylindrical and toroidal coordinates have been used, and realistic three-dimensional simulations of the whole torus are now within reach.

However, such sophisticated models necessarily involve a relatively large number of control parameters (the Larmor radius, the aspect ratio, the temperature and density gradients, the collisional dissipation, etc.). Since each large-scale simulation requires several tens of hours on a typical supercomputer, a systematic scan of the parameter space is obviously not feasible. On the other hand, even simple models retain some of the main features of drift turbulence, while depending on a smaller number of free parameters. It is therefore possible to perform a systematic analysis of some specific effect, and gain some insight into its repercussions on the turbulent dynamics.

Perhaps the simplest model of drift turbulence is the Hasegawa–Mima (H–M) equation (Hasegawa and Mima 1978), which is derived under several, more or less restrictive, assumptions: cold ions, a perfectly adiabatic response for the electrons,

* Present address: Laboratoire de Physique des Milieux Ionisés, Université Henri Poincaré, 54506 Vandoeuvre-les-Nancy, France.

and purely two-dimensional dynamics. However simple, this equation can have surprisingly rich turbulent solutions, which makes an analytical approach extremely difficult. Under the assumption of homogeneous and isotropic turbulence, and local interactions in wavenumber space, inertial ranges can be determined following the guidelines of Kolmogorov's theory of hydrodynamic turbulence (Ottaviani and Krommes 1992). Numerical results have shown the existence of these inertial ranges, although the actual slopes of the energy spectra are more difficult to determine with precision (Fyfe and Montgomery 1979; Hasegawa et al. 1979; Larichev and McWilliams 1991; Kukharkin et al. 1995; Watanabe et al. 1997).

Most numerical work so far has concentrated on homogeneous and isotropic turbulence. Anisotropy can arise, for example, from the existence of an equilibrium density gradient, which allows linear waves to propagate in the direction normal to the density gradient (drift waves). Linear wave effects can thus compete with nonlinear ones, and may have a significant impact on the turbulent dynamics (Rhines 1975; Maltrud and Vallis 1991; Kukharkin and Orszag 1996). These phenomena are studied in the present paper for the case of slowly decaying turbulence. Results show that wave effects do indeed modify the isotropic spectra. In some extreme cases, the turbulent energy transfer is virtually halted, and the spectrum is 'squeezed' into a narrow band in wavenumber space.

Finally, we note that the H–M equation is almost identical in structure to the Charney equation, which describes two-dimensional fluid turbulence in a rotating frame (Horton and Hasegawa 1994) (its main application is to planetary atmospheres). The analogues of drift waves are then Rossby waves. Most of the results obtained in this paper can be easily transposed to the Charney equation.

2. Model equation and previous results

In suitable units, the H–M equation is

$$\frac{\partial}{\partial t}(\nabla^2\phi - \phi) + J(\phi, \nabla^2\phi) + \beta \frac{\partial \phi}{\partial x} = 0, \tag{1}$$

where J is the two-dimensional Jacobian, defined as $J(a,b) = a_x b_y - a_y b_x$. Space is normalized to the ion Larmor radius $\rho_s = (T_e\, m_i)^{1/2}/eB$ and time is normalized to a/c_s, where $c_s = (T_e/m_i)^{1/2}$ is the sound speed and a is the size of the system. T_e and e are respectively the electron temperature and charge, while m_i is the ion mass. The electrostatic potential $\phi(x,y,t)$ is measured in units of $(T_e/e)\,\rho_s/a$. This normalization will be used throughout the text and in all figures, except where otherwise stated.

Equation (1) contains only two dimensionless parameters : $A = a/\rho_s$ represents the size of the system, measured in Larmor radii ; $\beta = a/L_n$ measures the relative importance of wave effects. L_n is a typical scale of variation of the equilibrium density profile, which is directed along the y axis. Note that (1) reduces to the two-dimensional Navier–Stokes equation for $\beta = 0$ and $k \gg 1$. The actual quantity transported by the flow is $W = \nabla^2\phi - \phi$. In this paper, we refer to W as the 'generalized vorticity' and to $\zeta = \nabla^2\phi$ as simply the 'vorticity', according to standard usage. The linear limit of (1) is equivalent to the evolution of a collection of independent drift waves obeying the (dimensionless) dispersion relation $\omega_{\mathbf{k}} = \beta k_x/(1+k^2)$. The computational box is periodic in the x direction ($0 < x < a$) and finite in y ($-\frac{1}{2}a < y < \frac{1}{2}a$; both ϕ and W vanish at $y = \pm\frac{1}{2}a$). Such boundary conditions

https://doi.org/10.1017/S002237789900759X Published online by Cambridge University Press

are similar to those that would be used in the case of cylindrical geometry, where only one coordinate (the azimuthal angle) is periodic, while the other (the radius) is finite. Our choice can thus be viewed as a 'pseudocylindrical' geometry, in which the correct boundary conditions are used but the curved metric is neglected. Furthermore, a dissipative term, of the form $-\nu\nabla^4 W$ (hyperviscosity), is added to the right-hand side of (1) to control the numerical noise at small wavelengths, although no forcing is included at this stage (freely decaying turbulence).

Anisotropy is introduced in (1) by the different boundary conditions and, more importantly, by the presence of the wave term proportional to β. Like the two-dimensional Navier–Stokes equation, the H–M equation possesses two inviscid quadratic invariants, the average energy E and the average enstrophy $\boldsymbol{\Omega}$:

$$E = \frac{1}{a^2}\int_a\int_a [(\boldsymbol{\nabla}\phi)^2 + \phi^2]\, d\mathbf{r}, \tag{2}$$

$$\boldsymbol{\Omega} = \frac{1}{a^2}\int_a\int_a [(\nabla^2\phi)^2 + (\boldsymbol{\nabla}\phi)^2]\, d\mathbf{r}. \tag{3}$$

We now briefly review the results of Kolmogorov's theory of homogeneous, isotropic turbulence applied to the H–M equation (Kraichnan and Montgomery 1980; Ottaviani and Krommes 1992). However, it should always be kept in mind that these results are in principle only valid for stationary driven-damped systems, in which energy and enstrophy are injected (and dissipated) at a constant rate. Their relevance to the slowly decaying case treated here is therefore questionable, although inertial-range ideas can serve as a guideline to interpret the numerical results of decaying experiments.

When $k \gg 1$, (1) reduces to the Navier–Stokes equation. If the forcing is localized around a wavenumber k_f, Kolmogorov's theory predicts a direct cascade of enstrophy for $k > k_f$, and a inverse cascade of energy for $k < k_f$. Defining the potential spectrum $E_\phi(k)$ such that $\int_0^\infty E_\phi(k)\, dk = \sum_k |\phi_k|^2$, one obtains

$$E_\phi(k) \sim \epsilon^{2/3}\, k^{-11/3} \quad (k < k_f), \tag{4a}$$

$$E_\phi(k) \sim \eta^{2/3}\, k^{-5} \quad (k > k_f), \tag{4b}$$

where ϵ and η are the rates of transfer of energy and enstrophy respectively. Indeed, (4) yields the usual Kolmogorov expressions when written in terms of the energy spectral density $E(k)$ ($\int_0^\infty E(k)\, dk = \sum_k (1 + k^2)|\phi_k|^2$), i.e. $k^{-5/3}$ in the energy range and k^{-3} in the enstrophy range. When $k \ll 1$, the same dependence of $E_\phi(k)$ is obtained, although in this case the energy spectral density $E(k)$ will differ from the Navier–Stokes result.

Most numerical work has concentrated on the regime $\beta = 0$ (isotropy) and $k \ll 1$, since this is the case that differs significantly from the well-studied Navier–Stokes equation. The inverse energy cascade was studied by Kukharkin et al. (1995) and Watanabe et al. (1997) for the driven case with $k \ll 1 \ll k_f$, and the spectrum of (4a) was recovered within good approximation. It was also observed that the transfer of energy to wavenumbers smaller than unity is significantly reduced, so that the spectrum has a peak at $k \approx 1$, and displays an ordered structure in real space ('quasicrystallization'). The direct enstrophy cascade was investigated by Larichev and McWilliams (1991) for weakly decaying turbulence. An energy spectrum $E \sim k^{-6}$ was observed (note that for $k \ll 1$ the energy and potential spectra have the same k dependence, i.e. $E(k) \sim E_\phi(k)$), which is somewhat steeper

than the prediction of (4b). It must be said, however, that spectra steeper than the Kolmogorov law are also usually observed in the enstrophy range of Navier–Stokes simulations (McWilliams 1984; Legras et al. 1988).

The case $\beta \neq 0$ (and $k \gg 1$) was studied by Rhines (1975) and Maltrud and Vallis (1991) in the context of geophysical fluid dynamics. Note, however, that in these studies the term $\partial\phi/\partial t$ is missing from (1), so that the dispersion relation becomes $\omega = \beta k_x/k^2$, which is dispersive for all wavenumbers, unlike (1). The two models become identical in the limit $k \gg 1$, but differ significantly when $k \ll 1$. Comparing the relative strength of the nonlinear and wave terms, Rhines points out that the transition between turbulent and wave-like motion should occur at

$$k_\beta = \left(\frac{\beta}{U}\right)^{1/2}, \tag{5}$$

with turbulence dominating for $k > k_\beta$ and waves dominating for $k < k_\beta$. U is a typical velocity of the flow, for example the mean square velocity, $U^2 = \sum_k k^2|\phi_k|^2$. Numerical experiments were carried out with both low- and high-wavenumber forcing (Maltrud and Vallis 1991). In the former case, energy spectra significantly steeper than the Kolmogorov result k^{-3} were found for purely Navier–Stokes turbulence ($\beta = 0$), probably due to the presence of coherent vortices. For finite β, such vortices are destroyed, and the spectrum becomes closer to the k^{-3} law (although this effect seems to depend on the forcing and dissipation mechanisms, and sometimes *steeper* spectra are observed for a finite β). At the same time, the spectrum becomes anisotropic. For high-wavenumber forcing, the inverse cascade $k^{-5/3}$ was observed in the inertial range, and it appeared not to be affected by the value of β. The cascade is arrested at k_β, where wave motion becomes dominant. More recent results (Kukharkin and Orszag 1996) – obtained, however, with a slightly different model – combine the effect of both β and the domain size A. They suggest that zonal flows (i.e. elongated structures parallel to the x axis, caused by the wave term in (1)) may be driven unstable by taking a relatively large value of A, resulting in the formation of ring vortices.

The aim of the present paper is to confirm the above results for finite β, and to extend them to the case of slowly decaying turbulence. For example, the numerical results of Maltrud and Vallis (1991) for driven–damped turbulence are still not conclusive as to the effect of waves on the direct cascade. In comparison with the isotropic case, a finite β appears to generate either a steeper or a shallower spectrum, depending on external parameters such as the forcing and the large-scale dissipation. On the other hand, the study of decaying turbulence envisaged here has the advantage of reducing the number of external parameters that can influence the spectral properties. It is hoped that the results presented in this paper will help to characterize turbulent solutions of drift equations and to quantify more precisely the effect of linear waves on the turbulent dynamics.

3. Numerical results

The H–M equation (1) is solved numerically using a hybrid spline-spectral method, coupled to a leapfrog integrator in time. Typically a mesh 1024×1024 was used, except where otherwise stated.

First, we investigate the case $A = 2\pi$, and therefore $k > 1$. This is the regime most relevant to geostrophic turbulence (the Charney equation). If we transform

to a moving frame $x' = x + \beta t$, (1) becomes (omitting primes)

$$\frac{\partial}{\partial t}(\nabla^2\phi - \phi) + J(\phi, \nabla^2\phi) + \beta \frac{\partial \nabla^2\phi}{\partial x} = 0. \tag{6}$$

Comparing the relative strengths of linear and nonlinear terms, one finds that wave effect are important when $\beta \approx k\phi$. This defines another criterion for the transition from the turbulent to the wave-dominated regime:

$$k'_\beta = \frac{\beta}{\Phi}, \tag{7}$$

where Φ is a typical value of the potential, defined, for example, as $\Phi^2 = \sum_k \phi_k^2$. Again, turbulence should dominate for $k > k'_\beta$ and waves for $k < k'_\beta$. The latter estimate is more accurate than that provided by (5), since the non-dispersive part of the drift frequency has been eliminated by switching to a moving frame. This is particularly important for small wavenumbers, for which the drift frequency is entirely non-dispersive.

The initial condition is restricted to a narrow band of small wavenumbers $1 < k_x < 4$, $0.5 < k_y < 2$ (owing to our boundary conditions, half-integer wavenumbers also are present in the y direction). The numerical timestep and the hyperviscosity used in this group of simulations are $\Delta t = 0.0015$ and $\nu = 3 \times 10^{-10}$. The average energy and enstrophy – defined in (2) and (3) – initially present in the system are respectively $E = 0.24$ and $\Omega = 0.75$. The average eddy turnover time τ_E (characteristic timescale of the turbulence) is defined as

$$\tau_E = \left(\frac{1}{a^2} \int_a \int_a |\nabla^2\phi|^2 \, d\mathbf{r} \right)^{-1/2}, \tag{8}$$

and its value turns out to be $\tau_E \approx 1.3$ in our units (note that the 'absolute' time is plotted in the figures).

We first treat the isotropic case, $\beta = 0$. The spectrum rapidly broadens to higher wavenumbers, and, after a few eddy turnover times, a quasistationary spectrum is formed. The anisotropy of the turbulence can be quantified by comparing the average unidirectional potential spectra

$$\langle |\phi(k_x)| \rangle = \frac{1}{2\pi} \int_{-\pi}^{\pi} |\phi(k_x, y)| \, dy, \tag{9a}$$

$$\langle |\phi(k_y)| \rangle = \frac{1}{2\pi} \int_{0}^{2\pi} |\phi(k_y, x)| \, dx, \tag{9b}$$

where, for example, $\phi(k_x, y)$ is obtained from $\phi(x, y)$ by Fourier transforming over x. Since the initial spectrum was localized at small wavenumbers, we expect the results from the direct enstrophy cascade to be more relevant to this case. According to (4b), and taking into account the definition of E_ϕ, the spectrum of the potential should be proportional to k^{-2} for both directions, since we are in the isotropic case.

The numerical results show that the spectrum is indeed isotropic and approximately follows a power law, although the slope is considerably steeper than that predicted by Kolmogorov's theory (Fig. 1). The exponent is measured to be roughly -2.7 for both directions. This would give $E_\phi(k) \sim k^{-6.4}$, which is to be compared with the k^{-5} of (4b). Again, it must be noted that spectra steeper than Kolmogorov's prediction have frequently been observed in simulations of both the Navier–Stokes

https://doi.org/10.1017/S002237789900759X Published online by Cambridge University Press

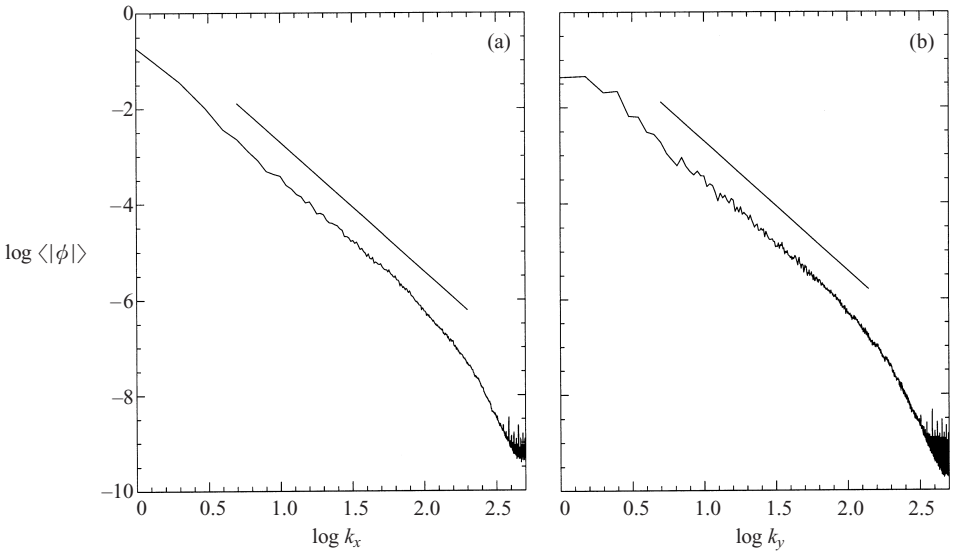

Figure 1. Unidirectional potential spectra for (a) k_x and (b), k_y for $\beta = 0$ and $A = 2\pi$. The straight line has a slope equal to -2.7. Logarithms are to base 10.

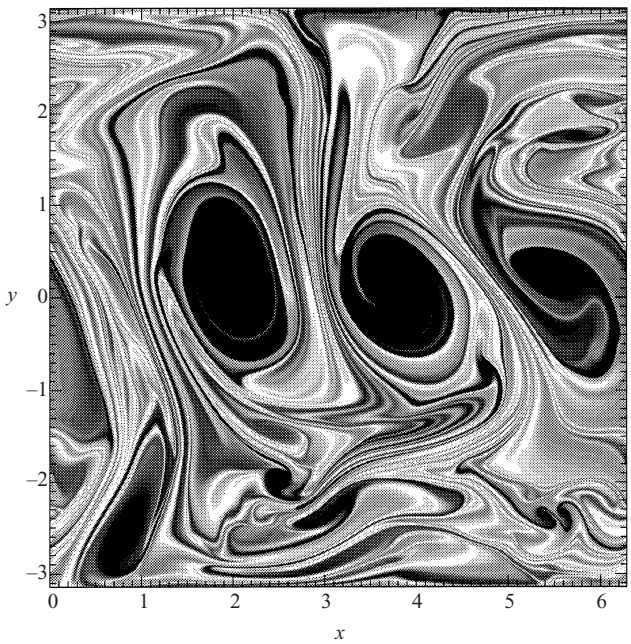

Figure 2. Shaded plot of the vorticity $\zeta = \nabla^2\phi$ for $\beta = 0$ and $A = 2\pi$.

and Hasegawa–Mima equations. This steepening is often attributed to the presence of 'coherent structures' (long-lived vortices) in the flow. Large vortices are indeed observed in the vorticity plot (Fig. 2). Another way to quantify the departure from Kolmogorov behaviour is to consider the kurtosis, which is defined, for a generic

https://doi.org/10.1017/S002237789900759X Published online by Cambridge University Press

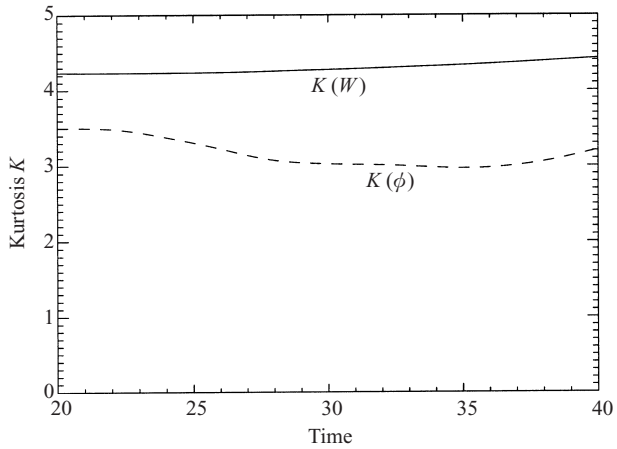

Figure 3. Time histories of the generalized vorticity kurtosis $K(W)$ (solid line) and potential kurtosis $K(\phi)$ (dashed line) for the case $\beta = 0$ and $A = 2\pi$.

function $f(x, y, t)$, as

$$K(f) = \frac{\langle f^4 \rangle}{\langle f^2 \rangle^2}, \tag{10}$$

where the angular brackets here indicate the area average. The kurtosis is equal to 3 for a Gaussian-distributed random variable. A kurtosis larger than 3 has been found to be often accompanied by steep spectra (Maltrud and Vallis 1991), and our results confirm this trend for the generalized vorticity kurtosis $K(W)$ (Fig. 3). The potential kurtosis $K(\phi)$ is instead much closer to its Gaussian value, again in agreement with previous simulation results.

The large vortices appearing in the isotropic case (Fig. 2) are destroyed even for moderate values of β, as shown in the shaded plot of the generalized vorticity (Fig. 4). A large vortex still survives for $\beta = 0.5$, while for $\beta = 2$ only small vortices are present. For $\beta = 5$, the flow is clearly anisotropic, and is dominated by elongated structures parallel to the direction of wave propagation ('zonal flows'). It therefore appears that an intermediate regime exists for moderate values of β, in which the flow is still isotropic, but large coherent structures are suppressed. This conclusion is supported by the potential spectrum for $\beta = 2$ (Fig. 5), which is indeed almost isotropic and virtually indistinguishable from the $\beta = 0$ case.

Next, we investigate the case of a strong β effect, by running three cases with $\beta = 10$, 20 and 40. The value of k_β, the wavenumber below which wave effects are important (see (5)) is respectively $k_\beta \approx 5$, 7 and 10, whereas (7) yields $k'_\beta \approx 3$, 6 and 12. The initial condition is the vorticity field obtained from the isotropic simulation at a time when the quasistationary state has already been obtained. After switching on the β effect, the spectrum becomes clearly anisotropic, steeper in k_x and shallower in k_y, as shown in Fig. 6 for $\beta = 10$ (the cases $\beta = 20$ and 40 are virtually identical). It appears that nonlinear transfer to high values of k_x is inhibited by the strong wave effect, so that the spectrum retreats to smaller wavenumbers. This does not happens for the k_y spectrum, which remains broad, while the slope of the inertial range becomes closer to -2, the value predicted by Kolmogorov's theory. This behaviour can be understood by noting that the wave term in (1) has the effect of breaking vortices along the x axis, thus reducing their

https://doi.org/10.1017/S002237789900759X Published online by Cambridge University Press

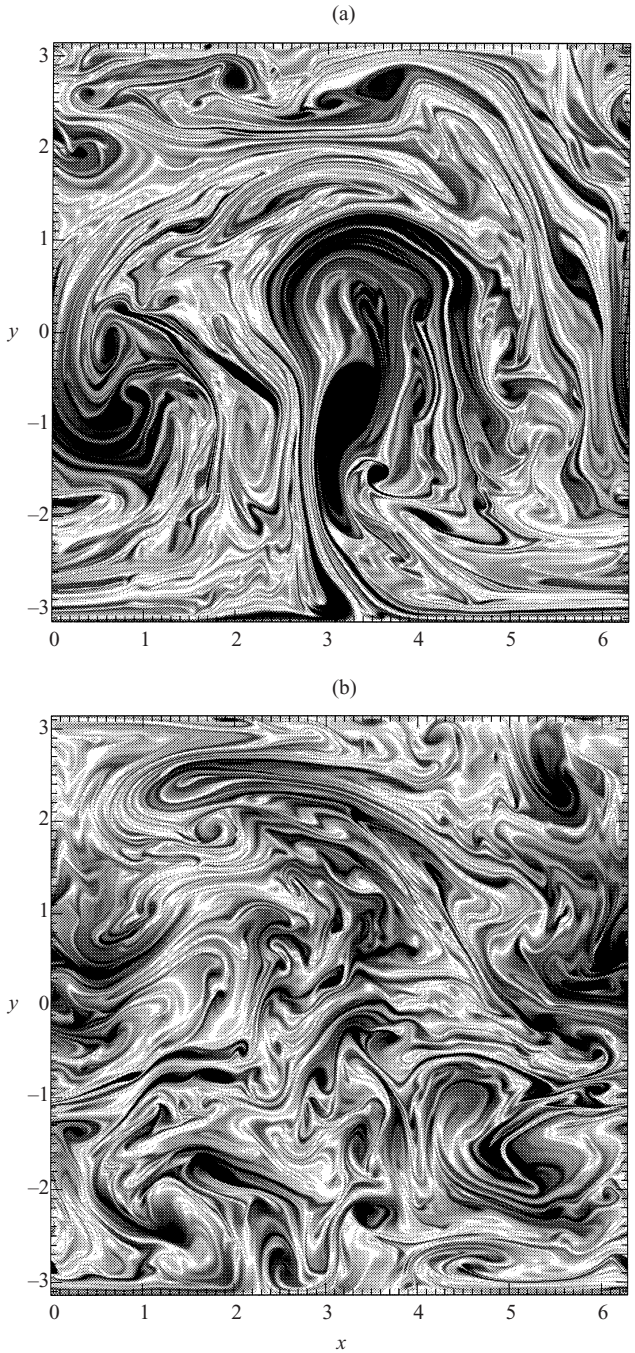

Figure 4. Shaded plots of the vorticity $\zeta = \nabla^2\phi$ for $A = 2\pi$ and (a) $\beta = 0.5$ and (b) $\beta = 2$.

https://doi.org/10.1017/S002237789900759X Published online by Cambridge University Press

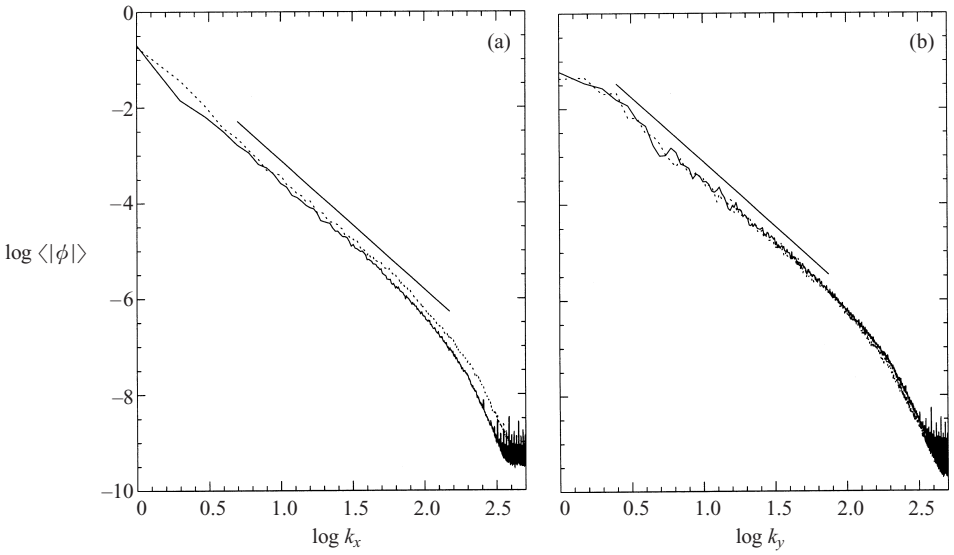

Figure 5. Unidirectional potential spectra for (a) k_x and (b) k_y, for $\beta = 2$ and $A = 2\pi$. The dotted line corresponds to the case of Fig. 1 ($\beta = 0$). The straight line has a slope equal to -2.7. Logarithms are to base 10.

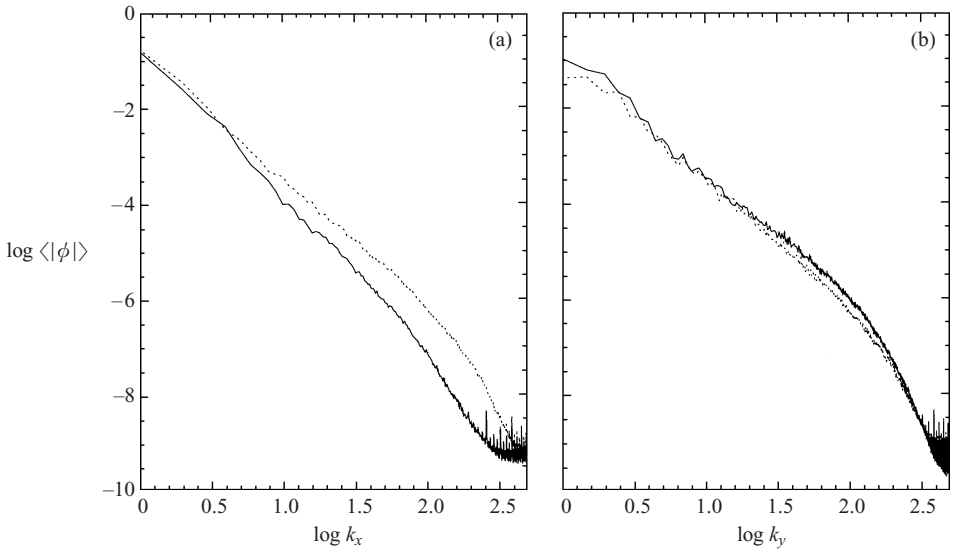

Figure 6. Unidirectional potential spectra for (a) k_x and (b) k_y, for $\beta = 10$ and $A = 2\pi$. The dotted line corresponds to the case of Fig. 1 ($\beta = 0$). Logarithms are to base 10.

size in the y direction but not in the x one. This results in the formation of zonal flows, clearly visible in the shaded plot of Fig. 7. The field becomes closer to a random field in the y direction, which is turn generates a Kolmogorov spectrum. At the same time, the vorticity kurtosis drops to a value close to 3, as expected for a Gaussian distribution (Fig. 8). The above results do not seem to depend on the actual value of β – at least when it is large enough for wave effects to play a

https://doi.org/10.1017/S002237789900759X Published online by Cambridge University Press

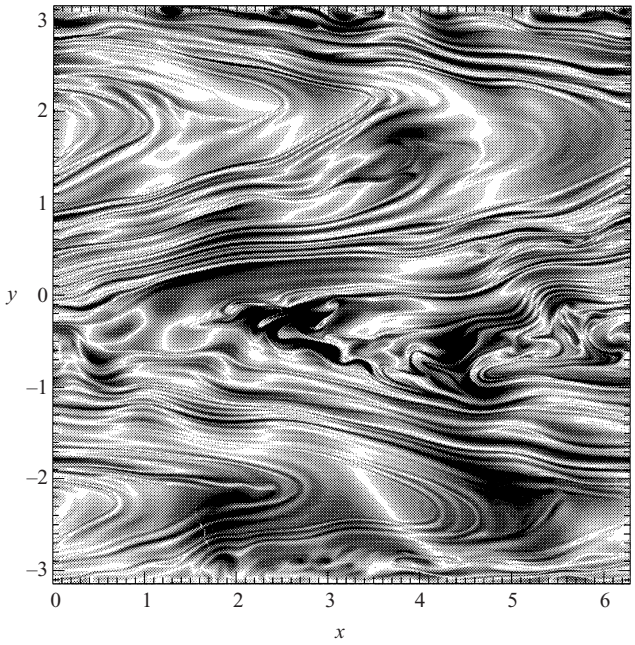

Figure 7. Shaded plot of the vorticity $\zeta = \nabla^2\phi$ for $\beta = 10$ and $A = 2\pi$.

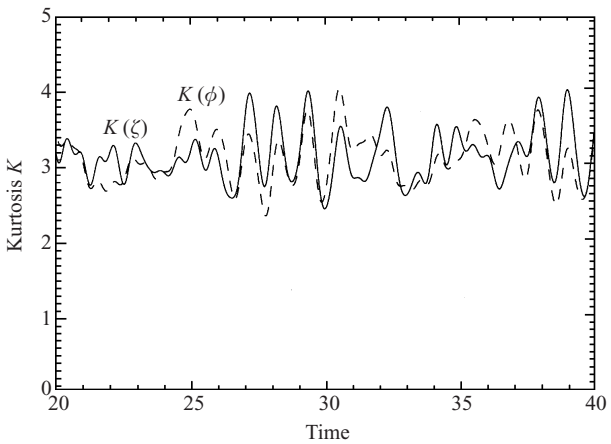

Figure 8. Time histories of the vorticity kurtosis $K(\zeta)$ (solid line) and potential kurtosis $K(\phi)$ (dashed line) for $\beta = 10$ and $A = 2\pi$.

significant role. In particular, the spectra appear to be virtually identical for the three values of β considered here.

It is interesting to evaluate the correlation functions of the potential in both directions, which are defined as

$$C(\delta x) = \langle \phi(x + \delta x, y)\ \phi(x, y) \rangle, \tag{11a}$$

$$C(\delta y) = \langle \phi(x, y)\ \phi(x, y + \delta y) \rangle, \tag{11b}$$

where the average is taken over both spatial variables. When the β effect is sufficiently strong, longer range correlations develop in x (Fig. 9a), while shorter correla-

https://doi.org/10.1017/S002237789900759X Published online by Cambridge University Press

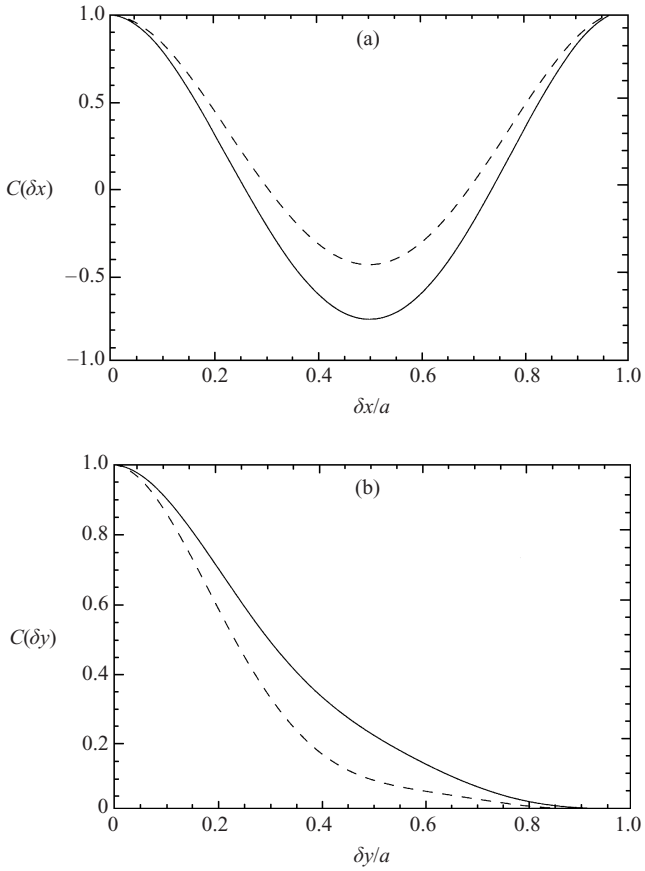

Figure 9. Correlation functions $C(\delta x)$ (a) and $C(\delta y)$ (b) for $A = 2\pi$ and $\beta = 0$ (solid line) and $\beta = 10$ (dashed line).

tions are observed in the y direction. This is another manifestation of the presence of zonal flows parallel to the x axis.

In another set of simulations, the β effect is introduced from the start, while again $A = 2\pi$. This time only four modes are initially excited, with wavenumbers $\mathbf{k} = (1, 0.5), (1, 1), (2, 0.5)$ and $(2, 1)$, and a mesh 256×256 was used, with hyperviscosity $\nu = 1.2 \times 10^{-7}$. Two cases are studied, with $\beta = 20$ and $\beta = 40$, corresponding to $k_\beta \approx 6.8$ and 9.6 respectively ($k'_\beta \approx 6.1$ and 12.2). Both initial conditions are therefore well inside the wave-dominated regime, and we suspect that nonlinear excitation will be rather inefficient. This is indeed the case, as shown in Fig. 10 for the $\beta = 40$ run: even for times large compared with the eddy turnover time ($\tau_E = 1.4$ in this case), the spectrum does not extend beyond k_β in either direction. The extent to which nonlinear transfer has been suppressed is quite remarkable, and results in all of the energy being 'squeezed' into a narrow band in wavenumber space. Moreover, the original modes are largely dominant, as is apparent from the power spectrum of the time history of the potential at a fixed point (Fig. 11a). This spectrum is strongly peaked at three frequencies, which closely match the linear frequencies of the four modes initially present in the system (it happens that two such frequencies have the same numerical value). For comparison, the same

https://doi.org/10.1017/S002237789900759X Published online by Cambridge University Press

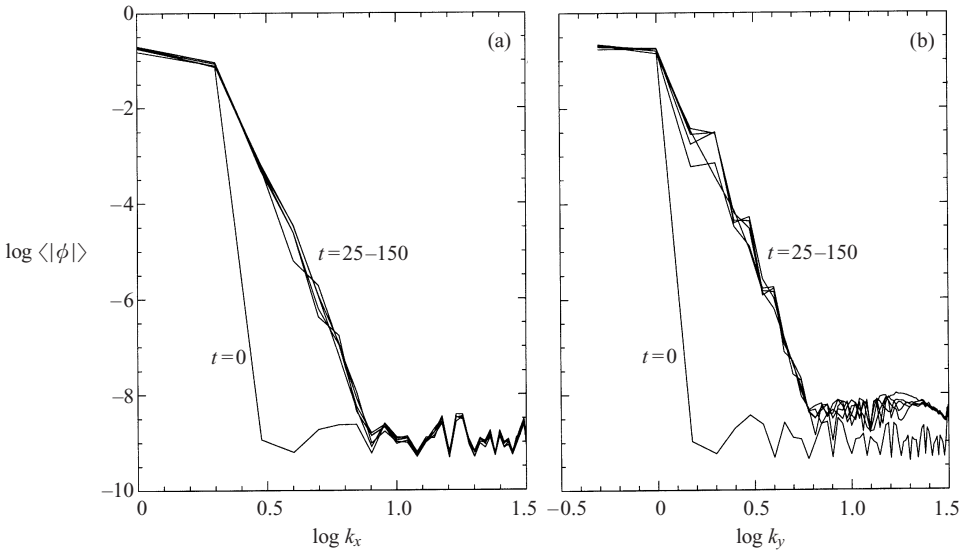

Figure 10. Unidirectional potential spectrum for (a) k_x and (b) k_y, for $\beta = 40$ and $A = 2\pi$, at different times of the evolution, from $t = 0$ to $t = 150$, at intervals of 25 units of time. Logarithms are to base 10.

spectrum is shown for a strongly turbulent case and the same value of β (Fig. 11b). In the latter case, the frequency spectrum is broader and extends to the small-frequency region, which reveals the presence of large wavenumbers, as expected from the dispersion relation $\omega_{\mathbf{k}} = \beta k_x/(1+k^2)$. Note that a cascade towards smaller frequencies was also predicted by Rhines (1975) (see also Horton and Hasegawa 1994) for resonant three-wave couplings (this will be analysed in the next section).

We now turn to the case $A \gg 1$, i.e. a domain size much larger than the Larmor radius, which is more relevant to the physics of magnetized plasmas. We first treat the isotropic case $\beta = 0$, for two values of the system size, $A = 30$ and $A = 60$. The eddy turnover time, computed from (8), is respectively $\tau_E \approx 3.5$ and $\tau_E \approx 4.2$. The shaded plot of the vorticity shown in Fig. 12 reveals that the characteristic size of the vortices scales with the Larmor radius ρ_s, and therefore decreases compared with the system size (Kukharkin et al. 1995). This effect is most evident from the plot of the correlation function $C(\delta x)$ shown in Fig. 13(a) for the three cases $A = 2\pi, 30$ and 60 (for clarity, in Fig. 13 lengths have been normalized to the system size a). The correlations go to zero for separations δx of the order of a few Larmor radii. The correlation function $C(\delta y)$ shown in Fig. 13(b), reveals a similar pattern. The potential spectrum for the case $A = 60$ is plotted in Fig. 14: it is isotropic and decays roughly as $k^{-2.7}$, as found for the case $A = 2\pi$. Indeed, Kolmogorov's theory predicts that the potential spectrum should not depend on the range of wavenumbers considered (and hence on the value of A). However, the spectrum is peaked at $k_{\mathrm{peak}} \approx 0.25$, which is larger than the fundamental wavenumber $2\pi/A \approx 0.10$. The vorticity kurtosis (Fig. 15) is again larger than the Gaussian value of 3, while the potential kurtosis is slightly smaller.

Next, we investigate the impact of wave propagation on the dynamics for large values of A. Three cases were studied, with $A = 60$ and $\beta = 0.2,\ 0.5$ and 5. The plots of the vorticity are shown in Fig. 16 for the latter two values of β, and reveal

https://doi.org/10.1017/S002237789900759X Published online by Cambridge University Press

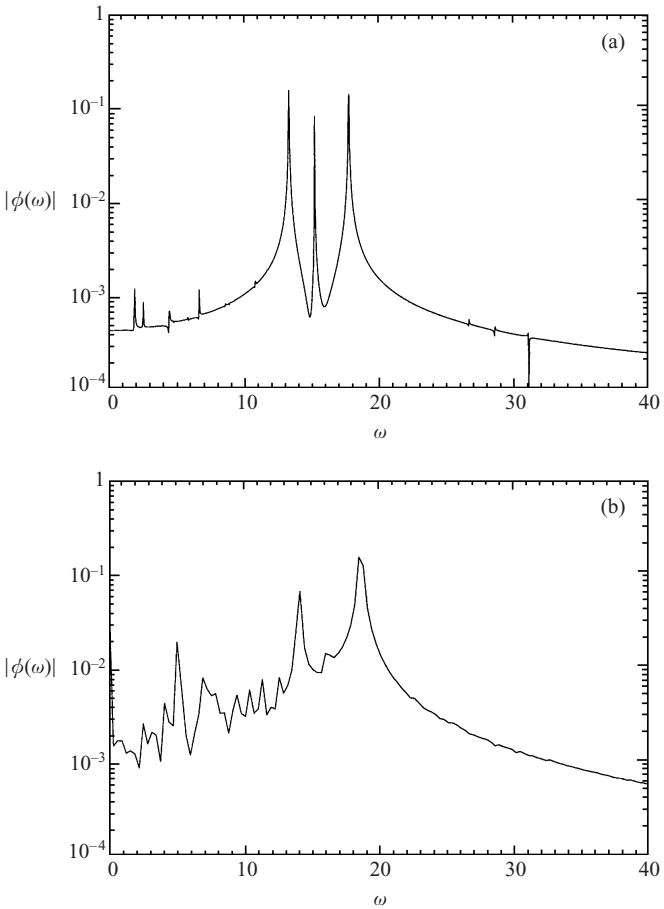

Figure 11. Power spectra of the potential at a fixed point (a) for the run of Fig. 10, with $\beta = 40$, and (b) for a run with same β but broad wavenumber spectrum. The peaks in (a) are located at $\omega = 13.3, 15.2$ and 17.8, and correspond to the linear frequencies.

a pattern similar to that detected for $A = 2\pi$. For $\beta = 0.2$, the wave effect is still small, and the resulting spectrum is close to the isotropic case. Taking large values of β leads to a flow largely dominated by zonal flows, with a spectrum steeper in the x direction (Fig. 14). In contrast to the $A = 2\pi$ case, where the y spectrum for large β was *shallower* than for $\beta = 0$, here it appears to have the same slope, or a slightly steeper one. Finally, the β effect brings both the vorticity and the potential kurtosis to a value close to 3 (Fig. 17).

We also note that, when longer wavelengths are considered, wave effects start to play a role at smaller values of β. Using (7), it is found that in the present case wave effects should be important for wavenumbers smaller than $k'_\beta \approx 0.4\beta$. For $\beta = 0.2$, we obtain $k'_\beta \approx 0.08$, while the fundamental mode is $k_0 \approx 0.1$, and this provides a reasonable estimate for the lowest β needed to introduce significant wave effects. It must be noted that, in our normalization, the potential is measured in units of $(T_e/e)\,\rho_s/a$: since the normalized potential is taken to be of the order of unity, it turns out that the real ϕ decreases with increasing size. In other words, our model assumes that the potential fluctuations scale with ρ_s/a. This is a

https://doi.org/10.1017/S002237789900759X Published online by Cambridge University Press

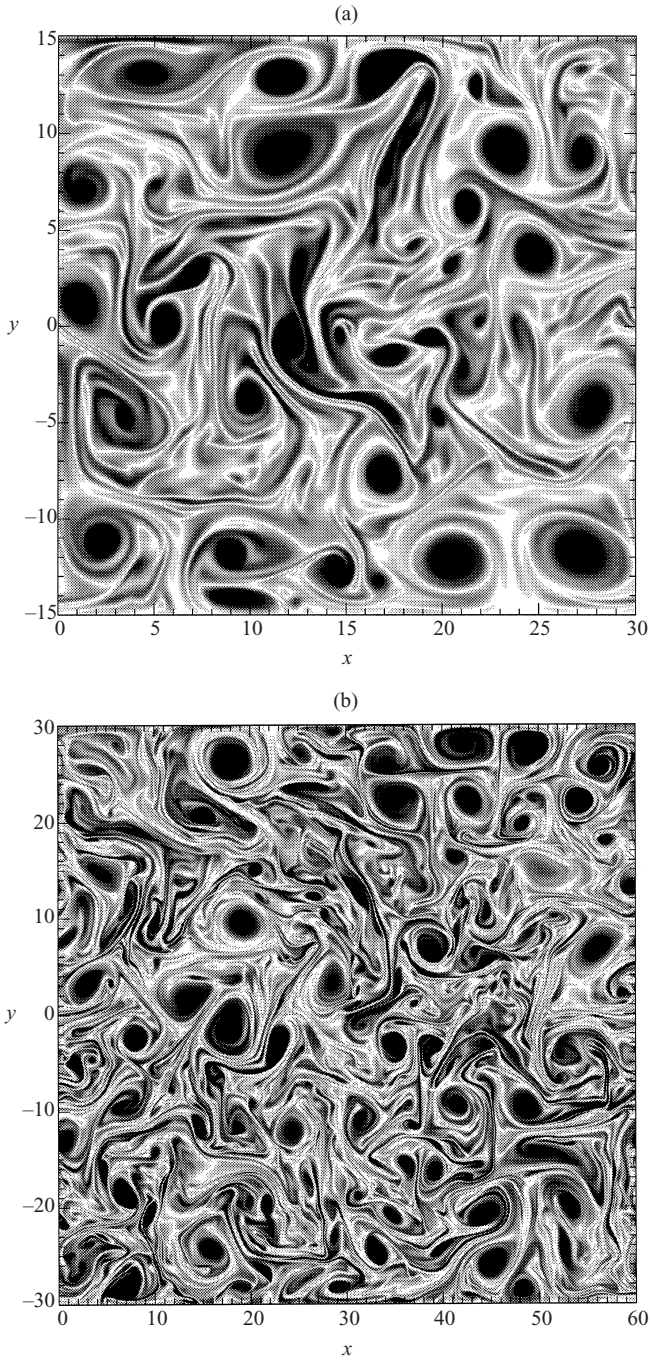

Figure 12. Shaded plots of the vorticity $\zeta = \nabla^2\phi$ for $\beta = 0$ and (a) $A = 30$ and (b) $A = 60$.

https://doi.org/10.1017/S002237789900759X Published online by Cambridge University Press

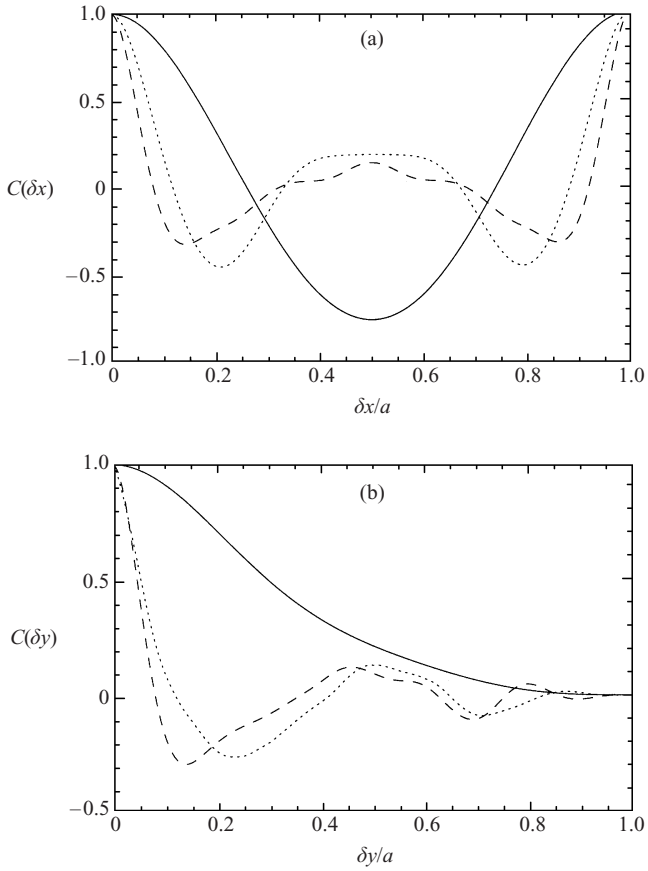

Figure 13. Correlation functions $C(\delta x)$ (a) and $C(\delta y)$ (b) for $\beta = 0$ and $A = 2\pi$ (solid line), $A = 30$ (dotted line) and $A = 60$ (dashed line). Space coordinates x and y are normalized to the system size a. The correlation functions are normalized so that $C(0) = 1$.

reasonable assumption, which can be derived on the basis of mixing-length arguments, assuming that the saturation level is proportional to the growth rate. Since for the ion-temperature-gradient instability (responsible for the destabilization of drift modes) the growth rate scales as ρ_s/a, one deduces that the potential should be of the same order. Alternatively, this fact implies that the two lengthscales entering our problem, namely the Larmor radius ρ_s and the inverse of k'_β, (7), are of the same order: $k'_\beta \rho_s \approx 1$. If this estimate is correct, one expects wave phenomena to play an important role on large-scale modes, which in turn may have an impact on the transport of mass and energy.

Finally, we perform a numerical experiment analogous to that presented in Fig. 10, but now with $A = 60$ and $\beta = 1$. Only four large-scale modes are initially present, with wavenumbers $\mathbf{k} \approx (0.1, 0.05)$, $(0.1, 0.1)$, $(0.2, 0.05)$ and $(0.2, 0.05)$, and mode amplitude equal to unity. The simulation is run for over 35 eddy turnover times ($\tau_E = 27$ in this case). Again, it is observed that nonlinear transfer to larger wavenumbers is arrested at $k'_\beta = \beta/\phi = 1$ (Fig. 18). In this simulation, as in most applications, lengthscales both larger and smaller than the Larmor radius are present simultaneously (specifically, we have $\rho_s k_{\min} \approx 0.05$ and $\rho_s k_{\max} \approx 10$). The numeri-

https://doi.org/10.1017/S002237789900759X Published online by Cambridge University Press

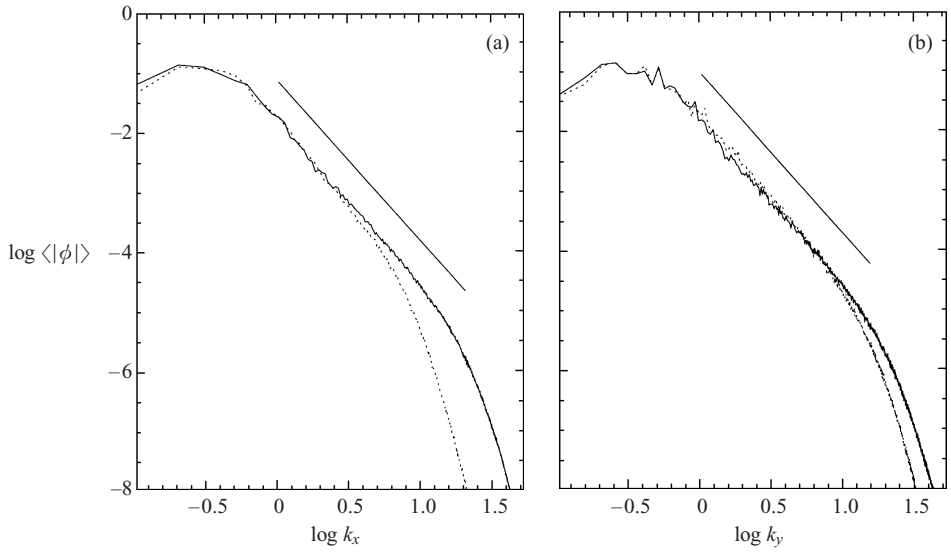

Figure 14. Unidirectional potential spectra for (a) k_x and (b) k_y, for $A = 60$ and $\beta = 0$ (solid line) and $\beta = 2$ (dotted line). The straight line has a slope equal to -2.7. Logarithms are to base 10.

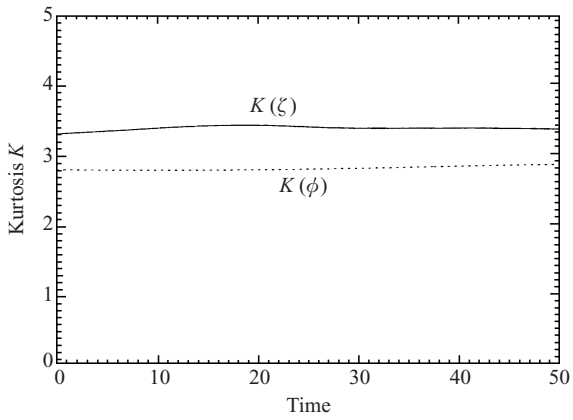

Figure 15. Time histories of the vorticity kurtosis $K(\zeta)$ (solid line) and potential kurtosis $K(\phi)$ (dotted line) for $\beta = 0$ and $A = 60$.

cal results thus suggest that small and large scales may be decoupled, small scales displaying turbulent dynamics, and large scales behaving essentially as weakly interacting linear waves. The boundary separating the different behaviours is given by k'_β, which, as discussed in the previous paragraph, turns out to be of order ρ_s^{-1} if the potential-fluctuation amplitude scales with the Larmor radius. It is important to note that the separation is given by the parameter k'_β, which is a measure of wave effects, rather than by the Larmor radius itself. It is only as a result of the scaling assumed for the potential that these two scales are comparable. If no waves are present, the Larmor radius itself does provide a barrier for nonlinear transfer, but this is a 'leaky' barrier. The point is that, for large-scale modes, nonlinear transfer takes place on a longer timescale (by a factor k^2), but is not completely arrested.

https://doi.org/10.1017/S002237789900759X Published online by Cambridge University Press

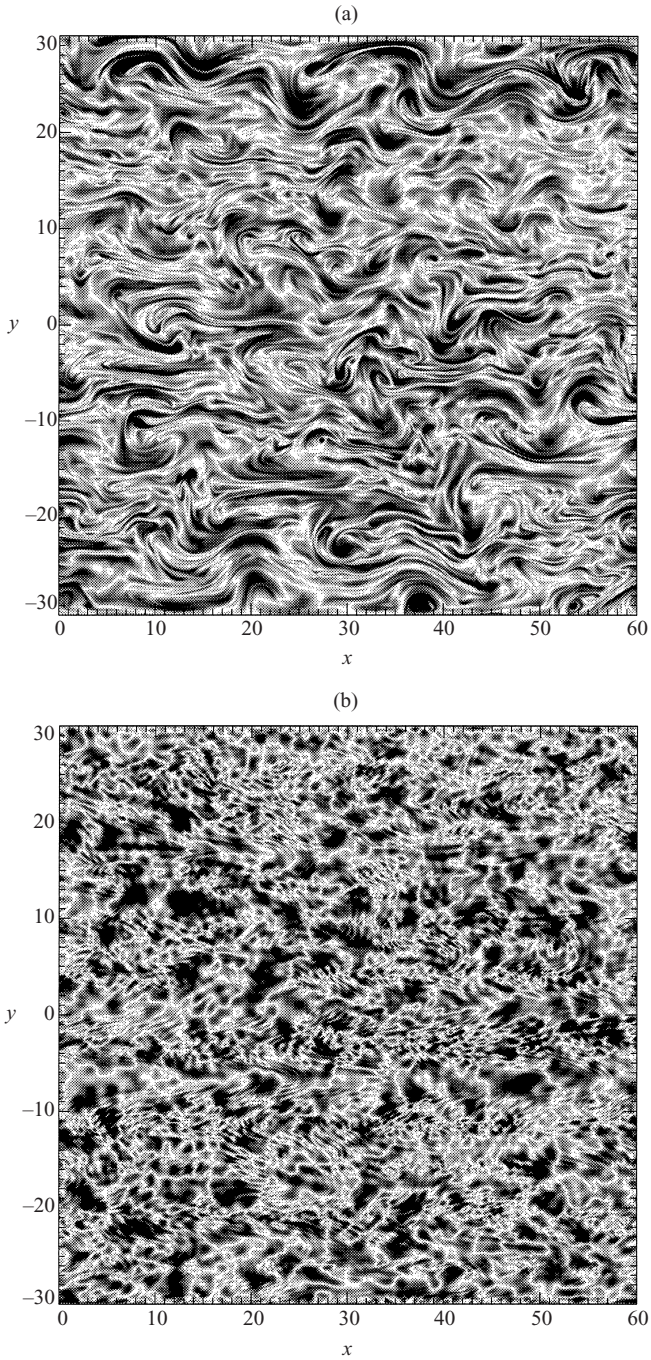

Figure 16. Shaded plots of the vorticity $\zeta = \nabla^2\phi$ for $A = 60$ and (a) $\beta = 0.5$ and (b) $\beta = 5$.

https://doi.org/10.1017/S002237789900759X Published online by Cambridge University Press

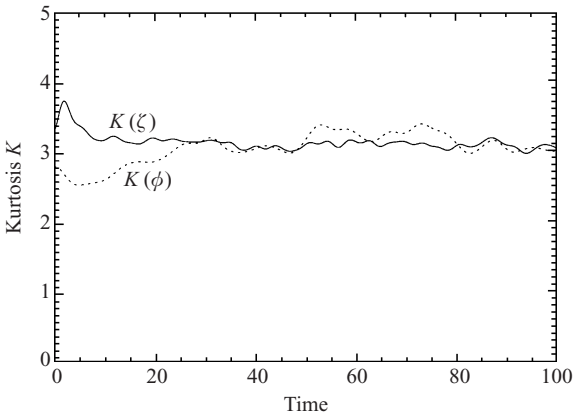

Figure 17. Time histories of the vorticity kurtosis $K(\zeta)$ (solid line) and potential kurtosis $K(\phi)$ (dotted line) for $\beta = 5$ and $A = 60$.

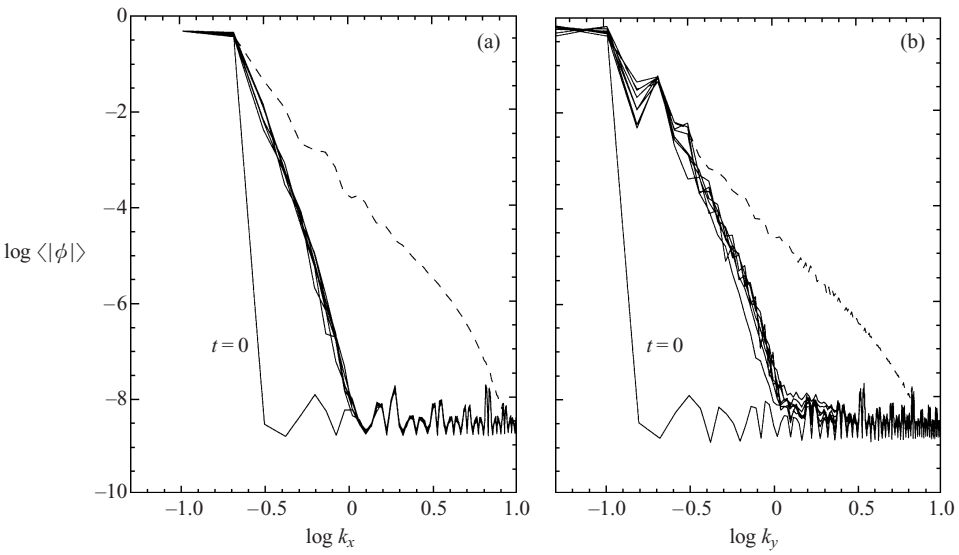

Figure 18. Unidirectional potential spectra for (a) k_x and (b) k_y, for $\beta = 1$ and $A = 60$, at different times of the evolution, from $t = 0$ to $t = 1000$ (solid line). The dashed line corresponds to the case $\beta = 0$, $A = 60$ at time $t = 400$. Logarithms are to base 10.

Figure 18 also shows the spectrum obtained with $\beta = 0$, which indeed extends to wavenumbers larger than unity. This effect was studied by Kukharkin et al. (1995) and Watanabe et al. (1997) for the inverse cascade, and was shown to lead to the formation of vortices with size of the order of the gyroradius ('quasicrystallization'). By contrast, the β effect seems to provide a much stronger barrier.

It must be added that the dynamics of drift waves for length scales much larger than the Larmor radius should be modelled by a slightly different equation, which also includes slow variations in the equilibrium electron temperature (see e.g. Spatschek et al. 1990; Horton and Hasegawa 1994; Kukharkin and Orszag 1996). The main difference from the standard H–M equation is the presence of a 'scalar

https://doi.org/10.1017/S002237789900759X Published online by Cambridge University Press

nonlinearity'

$$\alpha\phi\frac{\partial\phi}{\partial x}, \tag{12}$$

where $\alpha = \rho_s/L_T$, and L_T is the scale of variation of the electron temperature. Note that $\alpha \ll 1$, while $\beta \approx 1$. Comparing this new term with the standard nonlinear term (the Jacobian), we find that the scalar nonlinearity should play a role for wavenumbers of the order of or smaller than

$$k_\alpha = \alpha^{1/3}. \tag{13}$$

Note that, taking $\alpha = 0.001$ (consistent with tokamak parameters), yields $\rho_s k_\alpha = 0.1$, i.e. a wavelength still smaller than the machine size. Thus, for large enough structures, the scalar nonlinearity should be the dominant one, and may modify to some extent the previous numerical result. This interesting point will be the subject of further investigations.

4. Discussion

Much can be learned about nonlinear transfer by looking at a simplified model of mode coupling. Following the procedure outlined in Horton and Hasegawa (1994), let us suppose that the spectrum is dominated by three waves $\mathbf{k}_1, \mathbf{k}_2$ and $\mathbf{k}_3$ such that $\mathbf{k}_1 + \mathbf{k}_2 + \mathbf{k}_3 = 0$. From (1), it can be shown that the interaction of the three waves is described by the following set of equations:

$$\frac{d\phi_1}{dt} + i\omega_1\phi_1 = \Lambda^1_{2,3}\ \phi^*_2\ \phi^*_3, \tag{14a}$$

$$\frac{d\phi_2}{dt} + i\omega_2\phi_2 = \Lambda^2_{3,1}\ \phi^*_1\ \phi^*_3, \tag{14b}$$

$$\frac{d\phi_3}{dt} + i\omega_3\phi_3 = \Lambda^3_{1,2}\ \phi^*_1\ \phi^*_2, \tag{14c}$$

where the coupling coefficients $\Lambda^j_{l,m}$ are defined by

$$\Lambda^j_{l,m} = \frac{1}{2}\ \frac{k_l^2 - k_m^2}{1 + k_j^2}\ \mathbf{k}_l \times \mathbf{k}_m \cdot \hat{\mathbf{z}}. \tag{15}$$

We study the case where one of the modes is more highly populated than the others, so that we can linearize (11). We take

$$\phi_j = A_j(t)\exp(-i\omega_j t)\ , \quad j = 1, 3, \tag{16a}$$

$$\phi_2 = A_2\exp(-i\omega_2 t)\ , \quad A_2 = \text{const.} \tag{16b}$$

with $k_1 < k_2 < k_3$, and $A_1, A_3 \ll A_2$. The middle mode is thus more highly populated than the sidebands. From (14)–(16), we can obtain a second-order linear differential equation for $A_1(t)$ or $A_3(t)$, which has unstable solutions when

$$\Delta\omega^2 - 4\Lambda^1_{2,3}\Lambda^3_{1,2}|A_2|^2 < 0, \tag{17}$$

where $\Delta\omega = \omega_1 + \omega_2 + \omega_3$ is the frequency mismatch. It can be shown that $\Lambda^1_{2,3}\Lambda^3_{1,2} \geqslant 0$, so that an instability can actually exist. On the other hand, if modes 1 or 3 are highly populated, the system is unconditionally stable, showing that nonlinear transfer can only occur by exciting both a smaller and a larger wavenumber.

The system is unstable whenever the second term on the left-hand side of (17)

https://doi.org/10.1017/S002237789900759X Published online by Cambridge University Press

dominates, i.e. for high wavenumbers or large amplitudes. This is the case of turbulent coupling. In the opposite case, instability can occur only when $\Delta\omega \approx 0$, i.e. for a resonant three-wave process. Although both turbulent and resonant mode coupling scale in the same way (both occur on a time scale of order $(kU)^{-1}$), it is intuitive that the latter should be less efficient, since an additional constraint on the frequency mismatch must be satisfied. Broadly speaking, this is the reason why energy transfer is drastically slowed down when wave effects are important.

Now, if we consider the results shown in Figs 10 and 11, where only four long waves were initially present and $\beta = 40$, it can easily be seen that all possible combinations give a frequency mismatch of order β, while the Λ coefficients are all of order unity. In such a case, no instability can occur according to (14), which is in agreement with our numerical results. A similar conclusion is reached for the case of Fig. 18 ($A = 60$): the frequency mismatch is of order $\beta = 1$, while the Λ coefficients are proportional to the wavenumbers, and therefore small.

The above considerations on mode coupling can also be used to interpret our first set of simulations (Fig. 6), where the β effect was introduced after the wavenumber spectrum had already reached a quasistationary, isotropic state of the type $|\phi_k| \sim |\phi_0| k^{-\mu}$. Here ϕ_0 is a constant of order unity and the exponent μ was estimated to be close to 3. With these assumptions, the square root of the second term on the left-hand side of (17) scales as $\phi_0\, k^{-1}$ for large wavenumbers. If the interaction is non-resonant, $\Delta\omega \approx \omega_{\mathbf{k}} = \beta k_x/(1 + k^2)$, and this term scales as $\beta k_x/k^2$. As shown above, instability can arise only when the first term is smaller than the second. But, for large values of β, this can occur only when $k_x \approx 1$ and $k_y \gg 1$, because in this case $\Delta\omega \sim \beta k^{-2}$, while the other term scales as $\phi_0\, k^{-1}$. It is easy to show that in all other cases (e.g. $k_x \approx k_y \gg 1$), both terms scale in the same way, and no unstable solution is allowed for a large enough value of β.

The above discussion shows that a strong β effect tends to favour small wavenumbers in x and large wavenumbers in y, because only for these wavenumbers can turbulent, non-resonant mode coupling effectively take place. The numerical results presented earlier seem to support this conjecture. It must be noted that this type of mode interaction is highly non-local, contrary to Kolmogorov's assumption. Indeed, a typical wavenumber triad will be formed by two modes with $k_y \gg k_x \approx 1$ and one mode with $k_y \approx k_x \approx 1$, therefore coupling the large-scale isotropic flow with small-scale anisotropic zonal flows.

5. Conclusions

In this paper, we have discussed the impact of linear drift waves on the turbulent dynamics of the Charney–Hasegawa–Mima equation. Numerical experiments have been carried out in a slowly decaying regime with no external forcing. When no linear waves are present, and $A = 2\pi$, the wavenumber spectrum is isotropic, but considerably steeper than what is predicted by Kolmogorov's theory of stationary turbulence. Large-scale vortices are observed, together with high values of the vorticity kurtosis.

Increasing the relative importance of the wave term ('β effect') results in a substantial anisotropy of the flow, with the formation of elongated structures parallel to the direction of propagation of the waves (the x axis). The large vortices disappear as they are broken down by the shear effect introduced by the waves. The spectrum then becomes steeper in k_x (with almost no energy at large wavenumbers),

and shallower in k_y, getting closer to Kolmogorov's law. At the same time, the vorticity kurtosis drops to a value of approximately 3, expected for a random Gaussian variable.

When large values of β are introduced right from the beginning of the run, and the spectrum is initially localized to small wavenumbers, turbulent energy transfer is almost entirely inhibited. The spectrum remains confined to a narrow band of small wavenumbers for long times, and the dynamics is virtually linear. In this case, wave effects virtually decouple the dynamics of small and large scales.

For larger systems, $A = 30$–60, and $\beta = 0$, it has been shown that the vortex size scales with the Larmor radius ρ_s. The spectrum is peaked at wavenumbers $\rho_s k \approx 0.25$, but otherwise its slope does not depend on the size of the system, in agreement with Kolmogorov's theory of isotropic turbulence for the H–M equation. The flow is modified even at moderate values of β, developing an anisotropic structure similar to that already described for the case $A = 2\pi$. The results confirm that wave effects can play a significant role when the size of the system is large compared to the Larmor radius.

The numerical results have been interpreted using a simple model of nonlinear coupling among three waves. It has been shown that energy transfer can occur through either a resonant or a non-resonant (turbulent) process. The resonant process is far less efficient, since the modes must satisfy a stringent condition on their frequencies. For large values of β, mostly resonant interactions occur, thus reducing nonlinear energy transfer. Only for modes with $k_y \gg k_x$ is non-resonant coupling allowed, and this provides a qualitative explanation for the observed anisotropic spectra.

In conclusion, the simulations presented in this paper provide further evidence that wave effects strongly modify the usual picture of homogeneous and isotropic turbulence. Since, for example, test-particle transport has been shown to be rather sensitive to the structure of the underlying turbulent fields (Manfredi and Dendy 1996, 1997), the effects described above may have an impact on the confinement of charged particles in fusion devices.

Acknowledgement

This work was partially funded by the Association EURATOM-DCU.

References

Connor, J. W. and Wilson, H. R. 1994 *Plasma Phys. Contr. Fusion* **36**, 719.
Fyfe, D. and Montgomery, D. 1979 *Phys. Fluids* **22**, 246.
Hasegawa, A. and Mima, K. 1989 *Phys. Fluids* **21**, 87.
Hasegawa, A., Maclennan, C. G. and Kodama, Y. 1979 *Phys. Fluids* **22**, 2122.
Horton, W. and Hasegawa, A. 1994 *Chaos* **4**, 227.
Kraichnan, R. H. and Montgomery, D. 1980 *Rep. Prog. Phys.* **43**, 548.
Kukharkin, N. and Orszag, S. A. 1996 *Phys. Rev.* **E54**, 4524.
Kukharkin, N., Orszag, S. A. and Yakhot, V. 1995 *Phys. Rev. Lett.* **75**, 2486.
Larichev, V. D. and McWilliams, J. C. 1991 *Phys. Fluids* **A3**, 938.
Legras, B., Santangelo, P. and Benzi, R. 1988 *Europhys. Lett.* **5**, 37.
McWilliams, J. C. 1984 *J. Fluid Mech.* **146**, 21.
Maltrud, M. E. and Vallis, G. K. 1991 *J. Fluid Mech.* **228**, 321.
Manfredi, G. and Dendy, R. O. 1996 *Phys. Rev. Lett.* **76**, 4360.
Manfredi, G. and Dendy, R. O. 1997 *Phys. Plasmas* **4**, 628.

Manfredi, G. and Ottaviani, M. 1997 *Phys. Rev. Lett.* **79**, 4190.
Manfredi, G., Shoucri, M., Dendy, R. O., Ghizzo, A. and Bertrand, P. 1996 *Phys. Plasmas* **3**, 202.
Ottaviani, M. and Krommes, J. A. 1992 *Phys. Rev. Lett.* **69**, 2923.
Rhines, P. B. 1975 *J. Fluid Mech.* **69**, 417.
Spatschek, K. H., Laedke, E. W., Marquardt, Ch., Musher, S. and Wenk, H. 1990, *Phys. Rev. Lett.* **64**, 3027.
Sydora, R. D., Decyk, V. K. and Dawson, J. M. 1996 *Plasma Phys. Cont. Fusion* **38**, A281.
Waltz, R. E., Kerbel, G. D. and Milovich, J. 1994 *Phys. Plasmas* **1**, 2229.
Watanabe, T., Fujisaka, H. and Iwayama, T. 1997 *Phys. Rev.* **55**, 5575.